Research Square

Preprints are preliminary reports that have not undergone peer review.
They should not be considered conclusive, used to inform clinical practice,
or referenced by the media as validated information.

LncRNA NR_030777/DRP1 negatively regulates intercellular mitochondrial transfer in cobalt nanoparticles-induced neuronal damage

Yilong Chen
Fujian Medical University
Xiangyu Chang
Fujian Medical University
Jiamei Li
Fujian Medical University
Yilin Zhang
Fujian Medical University
Xinpei Lin
Fujian Medical University
Shangrong Jiang
Fujian Medical University
Cheng Chen
Fujian Medical University
Shengsong Lin
Fujian Medical University
Ling Lin
Fujian Medical University
Junjing Lin
Fujian Medical University
Zhenkun Guo
Fujian Medical University
Jinfu Zhou
Fujian Maternity and Child Health Hospital, Fujian Medical University
Hong Hu
Fujian Medical University
Guangxia Yu
Fujian Medical University
Wenya Shao
Fujian Medical University
Siying Wu

Fujian Medical University

Huangyuan Li

Fujian Medical University

Fuli Zheng

f.zheng@fjmu.edu.cn

Fujian Medical University

Research Article

Keywords: Cobalt nanoparticles, mitochondrial transfer, Tunneling nanotubes, non-coding RNA, DRP1

Posted Date: August 28th, 2026

DOI: https://doi.org/10.21203/rs.3.rs-10577780/v1

License: This work is licensed under a Creative Commons Attribution 4.0 International License.
Read Full License

Additional Declarations: No competing interests reported.

Abstract

Cobalt nanoparticles (CoNPs) are widely used in medical and renewable energy applications, with annual global consumption exceeding 0.2 million tons. However, CoNPs are neurotoxic. We recently found that intercellular mitochondrial transfer protects against CoNPs-induced neuronal apoptosis, and identified a long noncoding RNA NR_030777 as a regulator of mitophagy. Yet, whether NR_030777 governs mitochondrial transfer upon CoNPs exposure remains unknown. Here, we show that CoNPs trigger mitochondrial transfer from neuroglioma to neurons mainly via tunneling nanotubes (TNTs). Inhibition of TNT-mediated mitochondrial transfer exacerbated CoNPs-induced neuronal apoptosis, senescence, superoxide anion production, mitochondrial ROS and loss of mitochondrial membrane potential. Based on prior evidence of a direct physical interaction between NR_030777 and dynamin-related protein 1 (DRP1), we found that CoNPs suppressed DRP1 expression, and gain/loss-of-function studies established DRP1 as a negative regulator of TNT-mediated mitochondrial transfer. Genetic perturbation of NR_030777 suppressed mitochondrial transfer and worsened CoNPs-induced neurotoxicity. Rescue experiments confirmed that NR_030777 exacerbates apoptosis, oxidative stress, mitochondrial damage, and senescence by upregulating DRP1 to inhibit mitochondrial transfer. Collectively, this study demonstrates that lncRNA NR_030777 modulates DRP1 expression to inhibit TNT-mediated mitochondrial transfer, thereby exacerbating CoNPs-induced neurotoxicity. These findings uncover a novel epigenetic mechanism regulating intercellular mitochondrial communication and establish CoNPs as an environmental epigenetic toxicant that disrupts this protective process, opening new avenues for mechanistic and therapeutic research.

1. Introduction

CoNPs have been extensively utilized in diverse fields, including medicine, aerospace, and new energy batteries, owing to their advantageous properties [1]. Notably, over one million metal-on-metal (MoM) joint prostheses containing cobalt have been implanted worldwide, making these medical devices a significant source of endogenous CoNPs exposure due to the long-term wear [2]. Additionally, cobalt plays a critical role in the new energy sector, particularly in lithium-ion batteries, and has thus emerged as an increasingly important source of environmental and occupational exposure [3]. Global cobalt consumption increased substantially, driven largely by demand from the 3C (computer, communication, and consumer electronics) industry and the electric vehicle sector, rising from 75,000 tons in 2011 to 141,000 tons in 2020, with an average annual growth rate exceeding 7% [4].

However, existing evidence has demonstrated that CoNPs were potentially hazardous to humans and animals. In a population-based cohort study, patients receiving cobalt-containing hip prostheses had mean blood cobalt concentrations of up to 1.5 μg/L, which was more than 4-fold higher than in the metal-on-polyethylene (MOP) control group, and these patients developed symptoms of neurological damage [5]. Our previous work further confirmed elevated blood cobalt levels (2.514 μg/L) in patients with MoM implants compared with control subjects (0.06 μg/L) [6]. Animal studies have also shown that cobalt derived from hip replacements entered systemic circulation and accumulated in peripheral organs

[7–9]. *In vitro* experiments indicated that CoNPs can also cross biological barriers and induce neuronal damage [10]. We also documented CoNPs-induced damage to the nervous system in animals, cells, and the model organism *Caenorhabditis elegans* [6, 11–16]. In summary, CoNPs are hazardous materials capable of inducing neural damage in populations through medical, occupational, and environmental exposure routes. Nevertheless, the mechanisms underlying CoNPs-induced neurotoxicity remain poorly understood.

Given that aging increases susceptibility to environmental insults, aging is characterized by the progressive accumulation of time-related changes, leading to increased susceptibility to disease and death [17]. The brain is particularly vulnerable to aging processes, as evidenced by the exponential increase in the incidence of neurodegenerative diseases such as Alzheimer's disease with advancing age [17]. CoNPs may exacerbate this age-related vulnerability. We recently reported that mitochondria derived from astrocytes can be transferred to neurons via tunneling nanotubes (TNTs) to mitigate CoNPs-induced neurotoxicity [18]. TNTs are channels for intercellular mitochondrial transfer between cells, typically rich in actin and supplemented with microtubules [19]. We recently found that CoNPs induce the production of cellular reactive oxygen species (ROS) and mitochondrial reactive oxygen species (mtROS), which in turn activate the downstream PI3K/AKT pathway, promote TNTs formation, and mitigate CoNPs-induced neurotoxicity and mitochondrial damage [14]. Furthermore, several studies have indicated that TNT-mediated mitochondrial transfer was regulated by Rho GTPase family proteins, including Cell Division Cycle Protein 42 (CDC42) [20] and Mitochondrial Rho GTPase 1 (Miro1) [21]. Interestingly, DRP1, a key regulator of mitochondrial fission, also belongs to the Rho GTPase family. Phosphorylation of DRP1 at Ser616 site (p-DRP1-Ser616) is known to promote its translocation to mitochondria and facilitate fission processes. However, whether DRP1 and its phosphorylated form modulate CoNPs-induced mitochondrial transfer via TNTs remains unclear.

Our group previously found that NR_030777 directly binds to DRP1 through tagged RNA affinity purification (TRAP) experiments [22]. As an important branch of epigenetics, lncRNAs are closely linked to cell differentiation, tumorigenesis and neurological diseases [23–25]. In earlier studies, we found that NR_030777 not only contributed to nervous system damage but also regulated DRP1 to promote mitochondrial fission [22, 26, 27]. Despite these advances, it remains unknown whether NR_030777 influenced DRP1-mediated mitochondrial transfer via TNTs or participated in CoNPs-induced neurotoxicity.

In this study, we aimed to elucidate the potential role of TNTs-mediated mitochondrial transfer in CoNPs-induced neuronal damage the molecular mechanisms involving NR_030777 and DRP1. To test this hypothesis, we employed a neuron-glia co-culture model and genetic/pharmacological manipulations of DRP1 and NR_030777. This study provides the first evidence linking lncRNA-mediated epigenetic regulation to intercellular mitochondrial transfer in environmental neurotoxicity. This study provided the first evidence linking lncRNA-mediated epigenetic regulation to intercellular mitochondrial transfer and its role in environmental toxicant-induced neurotoxicity.

2 Results

2.1. TNTs mediate intercellular mitochondrial transfer to protect against neuronal damage induced by CoNPs

To investigate the mechanism of intercellular mitochondrial transfer under CoNPs treatment, HT22 and Glioma261 co-cultures were treated with 30 μg/mL CoNPs for 24 h, with or without a 0.5 h pretreatment with LAT-B, nocodazole (both TNT inhibitors), or GW4869 (an extracellular vesicle inhibitor). Confocal microscopy was used to quantify mitochondrial transfer from Glioma261 to HT22 and the number of TNTs between heterotypic (Glioma261–HT22) and homotypic (Glioma261–Glioma261 or HT22–HT22) cells (Fig. 1A). Both LAT-B and nocodazole markedly suppressed mitochondrial transfer (Fig. 1B) and reduced the formation of heterotypic TNTs (Fig. 1C) as well as homotypic TNTs within each cell type (Fig. 1D–E). GW4869 also decreased mitochondrial transfer and heterotypic TNTs to some extent, but its effect was weaker; moreover, it increased homotypic TNTs under control conditions (Fig. 1E). These results confirm that TNTs serve as the primary route for CoNPs-induced mitochondrial transfer from glial cells to neurons.

We next examined the functional role of TNT-mediated mitochondrial transfer in CoNPs-induced neuronal injury. Co-cultures were pretreated with LAT-B prior to CoNPs treatment, and apoptosis as well as intracellular O_2^- levels were assessed by flow cytometry. Inhibition of TNTs by LAT-B significantly increased both early and late apoptosis in HT22 and Glioma261 cells compared to CoNPs treatment alone (Fig. 1F–H). Concurrently, O_2^- levels were elevated in both cell types (Fig. 1I–K), indicating aggravated oxidative stress upon TNTs inhibition. Collectively, these findings demonstrate that TNT-mediated intercellular mitochondrial transfer from Glioma261 to stressed HT22 neurons represents an adaptive protective response against CoNPs-induced neurotoxicity; blocking this process exacerbates neuronal damage.

2.2. Mitochondrial transfer via TNTs can resist mitochondrial toxicity caused by CoNPs

We further investigated the role of TNT-mediated mitochondrial transfer in mitochondrial damage caused by CoNPs. Compared to the control group, mtROS levels in HT22 were significantly elevated (Fig. 2A-C). Conversely, MMP in both cell types was markedly reduced in response to CoNPs treatment (Fig. 2D-F). These findings indicate that intercellular mitochondrial transfer via TNTs contributes to cellular resistance against CoNPs-induced apoptosis and diminishing MMP loss in Glioma261. Given that senescence-associated β-galactosidase (SA-β-gal) activity is a well-established biomarker of cellular senescence and constitutes a key indicator of neurodegeneration[31], we assessed cellular senescence in HT22 following CoNPs treatment. Notably, treatment with CoNPs for 24 h resulted in a dose-dependent increase in SA-β-gal-positive cells, demonstrating elevated senescent phenotypes (Fig. 2G-H).

2.3. CoNPs down-regulate DRP1 to promote mitochondrial transfer via TNTs

Having observed that TNTs mediated mitochondrial transfer from Glioma261 to HT22 after CoNPs treatment, we further examined the expression of DRP1 and p-DRP1 (Ser616). Glioma261 cells were treated with 0, 10, 20, and 30 μg/mL CoNPs for 24 h, and protein levels of total DRP1 and p-DRP1 (Ser616) were subsequently analyzed by Western blot (Fig. 3A). Western blot analysis of Glioma261 cells demonstrated that CoNPs treatment reduced the abundance of total DRP1, while concomitantly increasing p-DRP1 (Ser616) (Fig. 3B-C).

The aforementioned findings demonstrated that CoNPs treatment significantly reduced DRP1 protein abundance while enhancing mitochondrial transfer and TNT formation between Glioma261 and HT22. We then employed pharmacological inhibition and genetic overexpression of DRP1 to elucidate its functional role in these processes. Glioma261 cells were treated with the DRP1 inhibitor Mdivi-1 of varying concentrations for 24 h, and the optimal concentration was determined using CCK-8 and mitochondrial morphology assays (Fig. 3D–F). Mdivi-1 treatment resulted in a dose-dependent increase in mitochondrial branch length, with a statistically significant difference at the optimal concentration compared to the control group.

After inhibition of DRP1 in Glioma261 with 30 μM Mdivi-1 for 24 h, the cells were co-cultured with HT22 and treated with CoNPs for an additional 24 h. The number of transferred mitochondria and the number of TNTs between the two cell types, as well as within homotypic cells, were subsequently examined. Inhibition of DRP1 in Glioma261 by Mdivi-1 resulted in a statistically significant increase in mitochondrial transfer to HT22 and in the number of TNTs between the two cell types (Fig. 3G–I). However, no significant difference was observed compared to the CoNPs-treated group. Conversely, the number of TNTs between homotypic cells showed no significant difference (Fig. 3J-K).

To investigate the role of DRP1 in mitochondrial transfer and TNTs formation, we generated a DRP1-overexpressing Glioma261 cell line via plasmid transfection. These cells were co-cultured with HT22 and treated with CoNPs for 24 h, followed by staining with Actin-Tracker Red-555. Using confocal fluorescence microscopy, we quantified mitochondrial transfer from Glioma261 to HT22, as well as TNTs formed between Glioma261 and HT22 and those among homotypic cells. Overexpression of DRP1 in Glioma261 significantly reduced mitochondrial transfer to HT22 compared with control conditions (Fig. 3L-M). Correspondingly, the number of TNTs between Glioma261 and HT22 was also decreased (Fig. 3N). In contrast, DRP1 overexpression resulted in an increase in TNTs among homotypic Glioma261 (Fig. 3O-P).

2.4. NR_030777 overexpression down-regulates intercellular mitochondrial transfer induced by CoNPs, increases neuronal damage and mitochondrial toxicity, and up-regulates DRP1 protein levels

Increasing evidence suggested that long non-coding RNAs are the regulators of almost all cellular processes [32–35]. We have previously uncovered that NR_030777 plays an important protective role in paraquat-induced neural damage [26, 36]. Therefore, NR_030777 overexpression and knockdown were used to investigate whether NR_030777 regulates mitochondrial transfer via TNTs and participates in neural damage caused by CoNPs.

Treatment of Glioma261 with CoNPs for 24 h resulted in a significant downregulation of NR_030777 expression, as determined by qRT-PCR (Fig. 4A). To further investigate its functional role, an NR_030777 overexpression model was established in Glioma261 cells via plasmid transfection, which elevated NR_030777 expression by approximately 80-fold compared to the control group (Fig. 4B). The NR_030777-overexpressing Glioma261 cells were co-cultured with HT22 and exposed to CoNPs for 24 h. Confocal fluorescence microscopy was employed to quantify mitochondrial transfer from Glioma261 to HT22, as well as the number of TNTs formed between Glioma261 and HT22 cells and within each cell type (Fig. 4C). Notably, NR_030777 overexpression significantly attenuated CoNPs-induced mitochondrial transfer from Glioma261 to HT22, and this reduction was statistically significant (Fig. 4D). Furthermore, a marked decrease in the number of TNTs was observed between the two cell types, as well as among homotypic cells, under NR_030777 overexpression conditions (Fig. 4E-G). All changes were statistically significant.

To further elucidate the regulatory effect of NR_030777 overexpression on key proteins involved in TNTs formation, we examined changes in DRP1 and p-DRP1 (Ser616) levels in Glioma261. Compared with the control group, DRP1 expression exhibited an upward trend, whereas p-DRP1 (Ser616) showed a downward trend (Fig. 4H–J).

To determine whether TNTs-mediated mitochondrial transfer contributes to CoNPs-induced neuronal damage, we assessed apoptotic activity and oxidative stress levels. To optimize space in the main text, the original multicolor flow cytometry dot plots are presented in **Supplementary Figure S1**. The corresponding quantitative analyses are shown as statistical graphs below. NR_030777-overexpressing Glioma261 were co-cultured with HT22 and treated with CoNPs for 24 h. Apoptosis was evaluated using Annexin V-PE/7-AAD staining, which demonstrated a statistically significant increase in early apoptosis in both cell populations compared to the CoNPs-treated group (Fig. 4K-L). Concurrently, intracellular O_2^- levels, detected by DHE staining and flow cytometry, were significantly elevated (Fig. 4M-N). At the mitochondrial level flow cytometric analysis using MitoSOX Deep Red revealed a substantial increase in mtROS in both cell types following CoNPs treatment (Fig. 4O-P). Conversely, NR_030777 overexpression in Glioma261 resulted in a significant decrease in mitochondrial membrane potential (MMP), as measured by TMRE assay (Fig. 4Q-R).

2.5. NR_030777 inhibition increases intercellular mitochondrial transfer, alleviating CoNPs-induced mitochondrial damage

To further investigate the role of NR_030777, we established a knockdown model in Glioma261 using siRNA targeting NR_030777, which resulted in an approximately 70% reduction in expression compared to the control group (Fig. 5A). Subsequently, NR_030777-knockdown Glioma261 were co-cultured with HT22 and exposed to CoNPs for 24 h, followed by similar examination of mitochondrial transfer and the number of TNTs (Fig. 5B). NR_030777 knockdown significantly enhanced mitochondrial transfer from Glioma261 to HT22 compared to control conditions, while CoNPs treatment failed to further increase mitochondria transfer (Fig. 5C). Consistent with earlier findings, we observed a substantial increase in TNTs formation between Glioma261 and HT22, among homotypic Glioma261, and between HT22 in response to CoNPs treatment (Fig. 5D-F). Nevertheless, NR_030777 overexpression failed to change TNTs numbers between cells, compared with the relative CoNPs treatment in NC group.

Given the enhanced mitochondrial transfer capacity following NR_030777 knockdown, we next examined alterations in key mitochondrial dynamics regulators. Western blot analysis revealed that NR_030777 knockdown significantly decreased total DRP1 protein levels while simultaneously increasing p-DRP1 (Ser616) following 24 h treatment to 30 μg/mL CoNPs (Fig. 5G-I).

To evaluate the functional consequences of enhanced mitochondrial transfer, we assessed cellular apoptosis and oxidative stress parameters (Figure S2 A-B). NR_030777-knockdown Glioma261 and HT22 co-cultures treated with CoNPs for 24 h exhibited significantly increased early apoptosis in both cell populations compared to the CoNPs-only treatment group (Fig. 5J-K). Intracellular O_2^- levels showed a decreasing trend, though this did not reach statistical significance (Fig. 5L-M). At the mitochondrial level (Figure S2 C-D), NR_030777 knockdown significantly reduced mtROS production (Fig. 5N-O) and markedly improved MMP in both cell types compared to CoNPs-treated controls (Fig. 5P-Q).

(A) Successful construction of NR_030777 knockdown Glioma261 using siRNA. **(B)** Representative mitochondrial transfer images of co-culture of NR_030777-knockdown Glioma261 and HT22 for 24 h. **(C)** The number of mitochondria transferred from NR_030777-knockdown Glioma261 to HT22. **(D)** The number of TNTs between NR_030777-knockdown Glioma261 and HT22. **(E)** The number of TNTs between homotypic NR_030777-knockdown Glioma261 cells. **(F)** The number of TNTs between HT22 cells. **(G-H)** Quantitative analysis of DRP1 and p-DRP1 (Ser616) protein levels shown in (G). **(J-K)** Apoptosis levels in both cell populations in the co-culture system of HT22 and NR_030777-knockdown Glioma261 treated with CoNPs for 24 h. **(L-M)** Intracellular O_2^- levels in co-culture system after 24 h. **(N-O)** mtROS in HT22 and NR_030777-knockdown Glioma261 co-cultures following 24 h CoNPs treatment. **(P-Q)** MMP in co-culture system after 24 h CoNPs treatment. The original multicolor flow cytometry dot plots are presented in **Supplementary Figure S2**. Scale bar = 50 μm, inset scale bar = 25 μm. Compared with the control group; **P* < 0.05, ***P* < 0.05, ****P* < 0.05; compared with the CoNPs group, #*P* < 0.05, ## *P* < 0.01, ###*P* < 0.001. n = 3.

2.6. LncRNA NR_030777 targets DRP1 to suppress TNTs-mediated mitochondrial transfer and contributes to CoNPs-induced neurotoxicity

Our previous results demonstrated that both DRP1 and lncRNA NR_030777 negatively regulate TNTs-mediated mitochondrial transfer upon CoNPs treatment. Notably, we have previously shown through TRAP experiments that NR_030777 directly binds to DRP1, and our earlier study in paraquat-induced neurotoxicity revealed that NR_030777 modulates DRP1 expression [26]. However, it remains unclear whether NR_030777 exerts its regulatory function by targeting DRP1 in the context of CoNPs treatment. Therefore, we performed a rescue experiment to elucidate the functional interaction between NR_030777 and DRP1 and their role in CoNPs-induced neuronal damage. Specifically, we overexpressed NR_030777 in Glioma261 and inhibited DRP1 activity using Mdivi-1, followed by co-culture with HT22.

Mitochondrial transfer and TNTs formation were assessed using confocal microscopy (Fig. 6A). Notably, DRP1 inhibition reversed the suppression of mitochondrial transfer caused by NR_030777 overexpression, resulting in increased mitochondrial movement from Glioma261 to HT22 (Fig. 6B-C). Concomitantly, the number of TNTs between Glioma261 and HT22, as well as among homotypic cells, was significantly elevated compared to the NR_030777 overexpression group (Fig. 6D-E).

In line with these findings, we investigated the role of NR_030777/DRP1-mediated mitochondrial transfer via TNTs in cellular senescence induced by CoNPs. To this end, we conducted a rescue experiment and assessed senescence using the classical marker SA-β-gal (Fig. 6F). As anticipated, the rescue group exhibited a significant reduction in SA-β-gal positivity compared to the NR_030777 overexpression group, with levels approaching those observed in the control group (Fig. 6G).

We further evaluated the functional consequences of restored mitochondrial transfer using flow cytometry (Figure S3 A-D). Apoptosis analysis revealed a decrease in HT22 cell death upon DRP1 inhibition in NR_030777-overexpressing co-cultures (Fig. 6H-I). Conversely, intracellular O_2- levels were increased in both cell populations (Fig. 6J-K). At the mitochondrial level, mtROS production showed a downregulation (Fig. 6L-M), while MMP was notably enhanced compared to NR_030777-overexpressing cells without DRP1 inhibition (Fig. 6N-O).

These results demonstrate that NR_030777 negatively regulates TNTs-mediated mitochondrial transfer through a DRP1-dependent mechanism, and that modulation of this pathway significantly influences CoNPs-induced neuronal damage outcomes.

3. Discussion

With the increasing demand and application of CoNPs, their damage to the nervous system has attracted widespread attention. We found that NR_030777 negatively regulates the mitochondrial transfer of TNTs by upregulating DRP1 and participates in the neuronal damage caused by CoNPs. This is the first time that lncRNA has been found to be actively involved in mitochondrial transfer between neuronal cells and neuroglia. It is also novel that TNTs-mediated mitochondrial transfer via the NR_030777/DRP1 pathway contributes to neurological damage caused by CoNPs, an environmental toxicant.

This study discovered that TNTs mediate mitochondrial transfer and participate in CoNPs-induced neurotoxicity. The results indicate that compared with the vesicle inhibitor group and the control group, the number of transferred mitochondria decreased upon TNTs inhibition. Our results unveiled that TNTs are the primary means of mediating the mitochondrial transfer from glioma261 to HT22. This is consistent with the conclusion reported in previous studies that mitochondria can be delivered via TNTs in MSC cells [37–39]. Furthermore, we found that CoNPs treatment can increase the number of TNTs and transferred mitochondria. Next, we investigated whether TNTs-mediated mitochondrial transfer can play a role in CoNPs-induced neural damage. We observed that after blocking TNTs formation with TNTs inhibitors, CoNPs increased cell apoptosis and O_2^- levels, as well as mitochondrial ROS and MMP levels. Similarly, previous studies have observed that mitochondria are transferred from MSCs to PC12 cells via TNTs, and inhibition of TNTs also abolished the beneficial effects of MSCs on injured PC12 cells [40]. Thus, our results indicate that mitochondrial transfer via TNTs can alleviate CoNPs-induced neuronal toxicity and mitochondrial damage.

We have previously found that NR_030777 plays an important role in neural damage caused by environmental toxin paraquat through the regulation of mitophagy and cell cycle [22, 26]. Here, we show that DRP1 negatively regulates TNT-mediated mitochondrial transfer: its inhibition enhanced transfer, while its overexpression suppressed it. Crucially, rescue experiments confirmed that NR_030777 depends on DRP1 to suppress mitochondrial transfer, as DRP1 inhibition reversed the deficits caused by NR_030777 overexpression. Furthermore, CoNPs treatment promoted cellular aging and affected the aging-related marker by the NR_030777/DRP1 pathway, this result means that impaired mitochondrial transfer may not only worsen immediate neurotoxicity but also contribute to accelerated neuronal decline associated with aging, consistent with the known role of mitochondrial dysfunction in both toxicity and aging [17].

In other studies on lncRNA, additional lncRNAs, such as lnc-Gm10532 have also been found to play important roles in the nervous system [41], such as alleviating neuroinflammation via miR-671-5p/NF-κB pathway [42].

In a series of studies on NR_030777 by our group, we have found that NR_030777 can bind to DRP1[22, 26]. Interestingly, DRP1 and proteins that regulate mitochondrial transfer via TNTs belong to the Rho-GTPase family. First of all, we explored whether DRP1 regulates mitochondrial transfer via TNTs. We found that overexpression of DRP1 reduced mitochondrial transfer, while inhibition of DRP1 increased mitochondrial transfer. The results indicate that DRP1 negatively regulates mitochondrial transfer via TNTs. Next, by overexpressing NR_030777 and inhibiting DRP1 at the same time, we explored whether NR_030777 regulates DRP1-mediated mitochondrial transfer via TNTs. The results showed that NR_030777 upregulates DRP1, negatively regulates mitochondrial transfer via TNTs, and participates in CoNPs-induced neural damage. In summary, we found that lncRNA and mitochondrial dynamics are linked to mitochondrial transfer via TNTs upon CoNPs treatment. However, the mechanism between the downstream of DRP1 and TNTs is not clear yet. Moreover, most of the current research on TNTs is based

on *in vitro* experiments. Therefore, the downstream mechanisms of DRP1 and mitochondrial transfer through TNTs can be explored in future using *in vivo* models.

In summary, our research is the first to reveal the involvement of epigenetic mechanisms, mitochondrial fission, and mitochondrial transfer via TNTs involved in CoNPs-induced neural damage. Our findings provide a new theoretical basis for the protective effects of cell damage in the field of toxicology and offer new ideas and strategies for the prevention and control of neural damage caused by environmental hazards.

4. Materials and methods

4.1. Materials

CoNPs were obtained from Sigma-Aldrich (St. Louis, MO, USA), which have been characterized in our previous study [13, 18] (see **2.2** for details). Cell culture reagents were sourced as follows: high-glucose Dulbecco's modified Eagle's medium (DMEM), fetal bovine serum (FBS), penicillin-streptomycin solution, and 0.25% trypsin-EDTA, were acquired from Corning (Corning, NY, USA), Biological Industries (Kibbutz Beit Haemek, Israel), HyClone (Logan, UT, USA), and Gibco (Grand Island, NY, USA), respectively. Reagents for molecular biology were purchased as follows: TRIzol reagent, a reverse transcription kit, and a SYBR Premix Ex Taq fluorescence quantitation kit from Accurate Biotechnology Co., Ltd. (Hunan, China); primers from Sangon Biotech (Shanghai, China); small interfering RNA targeting NR_030777 (siNR_030777), an NR_030777 overexpression plasmid, and a mitochondria-targeted enhanced green fluorescent protein (mito-EGFP) lentivirus from Gene Pharma (Suzhou, China). Tetramethylethylenediamine (TEMED), sodium dodecyl sulfate (SDS), ammonium persulfate (APS), a 40% acrylamide solution, and a cell counting kit-8 (CCK-8) were obtained from Thermo Fisher Scientific (Waltham, MA, USA). An ECL developing reagent and an Annexin V/7-AAD Kit were sourced from BD Biosciences (San Jose, CA, USA). RIPA cell lysis buffer, a mitochondrial membrane potential assay kit (TMRE kit), and a dihydroethidium (DHE) probe were procured from Beyotime Institute of Biotechnology (Shanghai, China). A protease inhibitor was obtained from Solarbio Science & Technology Co., Ltd. (Beijing, China). MitoTracker Green FM and Mitochondrial Superoxide Indicators (MitoSOX Red) were acquired from Cell Signaling Technology (Danvers, MA, USA) and Dojindo Laboratories (Kumamoto, Japan), respectively. The following primary antibodies were used: rabbit anti-DRP1 and anti-phospho-DRP1 (Ser616) from Abcam (Cambridge, MA, USA); anti-β-ACTIN from ProteinTech Group (Wuhan, China); rabbit anti-Miro1 from BOSTER Biological Technology Co., Ltd. (Wuhan, China). Common solvents, including anhydrous ethanol, chloroform, and isopropyl alcohol (all analytical grade), were purchased from Sinopharm Chemical Reagent Co., Ltd. (Shanghai, China). 1st Strand cDNA Synthesis Kit was purchased from Accurate Biotechnology Co., Ltd (Hunan, China).

4.2. Cell Culture and Exposure

Mouse hippocampal neuronal cell line (HT22) and mouse glioma cells (Glioma261) were purchased from Cellverse (iCell) Bioscience Technology Co., Ltd. (Shanghai, China). The two cell lines have been

widely used and recognized in neurological and toxicological studies [28] To enable visualization of mitochondrial transfer from glial cells to neurons, Glioma261 cells were engineered to stably express EGFP-tagged mitochondria using a mito-EGFP lentivirus, generating a Glioma261-mito-EGFP cell line. Briefly, the lentiviral solution was diluted with complete medium at ratios of 1:10, 1:100, and 1:1000 to a total volume of approximately 1 mL, and polybrene was added to a final concentration of 5 μg/mL. The cells were incubated with the gradient-diluted virus at 37°C under 5% CO_2 for 24 h. After incubation, the lentivirus-containing medium was aspirated, and the cells were refreshed with new complete medium supplemented with 0.5 μg/mL puromycin for 96 h to select stably transduced cells. Following 96 h of selection with 0.5 μg/mL puromycin, the Glioma261-mito-EGFP cell line was successfully established, and the puromycin concentration was reduced by half for long-term maintenance.

All cells were cultured in a humidified incubator at 37°C with 5% CO_2 and grown in high-glucose DMEM supplemented with 10% fetal bovine serum (FBS), 100 U/mL penicillin, and 100 μg/mL streptomycin. To modulate gene expression, NR_030777 knockdown and overexpression were achieved using siRNA and plasmid constructs, respectively. DRP1 was overexpressed using a plasmid, and its activity was inhibited with Mdivi-1, a specific chemical inhibitor.

CoNPs have been thoroughly characterized in terms of particle size, zeta potential, and morphology, with spherical particles sizes ranging from 13.34 to 85.79 nm in size [13, 18]. CoNPs were prepared into a 1 mg/mL stock solution with deionized water, sonicated for 15 min, vortexed for 5 min, dispensed into 1.5 mL EP tubes, and stored in a refrigerator at -20°C. Before each experiment, the CoNPs stock solution was thawed and re-sonicated for 10 min to ensure uniform dispersion. Cells were exposed to CoNPs at concentrations of 0 ~ 30 μM for 24 h. The selected CoNPs doses were comparable to those in endogenous cobalt-exposed populations and have been shown to induce neurotoxicity [5].

4.3. Immunostaining

HT22 cells were co-cultured with Glioma261-mito-EGFP cells (established in our previous study [11]) until the cell density reached 50%. Cells were then fixed sequentially with Fixative 1 and Fixative 2, each for 20 min [29]. The microfilament Red fluorescent probe (Actin-Tracker Red-555) was added at a 1:200 dilution ratio and incubated for 30 min at room temperature. 200 μL of DAPI-containing antifade mounting medium was added in the dark, and samples were photographed using a laser confocal microscope. For MitoTracker staining, Glioma261-mito-EGFP cells were treated with Mdivi-1 for 24 h, followed by incubation with 200 nM MitoTracker Green FM in 5% CO_2 at 37°C for 30 min. Samples were then recorded using a Leica laser confocal microscope.

4.4. Western Blotting

Protein samples were extracted using RIPA lysis buffer. Then, 20 μg of protein were denatured, separated by SDS-PAGE, and then transferred to PVDF membranes (0.22 μm). The proteins were blocked with non-fat milk, incubated with a primary antibody overnight at 4°C, and incubated with the secondary antibody for an additional 1 h the next day. Protein images were captured using a Tanon 5200 Automatic

Chemiluminescence Image Analysis System (Shanghai, China), and gray values of proteins were analyzed using ImageJ software. Primary antibodies used in this study are listed in **2.1 Materials**.

4.5. Apoptosis Detection

HT22 cells were co-cultured with Glioma261-mito-EGFP cells, and then treated with 30 μg/mL CoNPs for 24 h. Both floating and adherent cells were collected, and the cell concentration was adjusted to 1×10^6 cells per mL. Cells were then incubated with Annexin-V-PE and 7-AAD for 1 h at 25°C in the dark, followed by flow cytometry (FACSCanto II, BD, USA) analysis within 15 min.

4.6. Cellular superoxide anion level Determination

HT22 cells were co-cultured with Glioma261-mito-EGFP cells and then treated with 30 μg/mL CoNPs for 24 h. After centrifugation at 300 ×g, cells were incubated with 10 μM dihydroethidium (DHE) at 37°C for 30 min. The intracellular superoxide anion (O_2^-) level was then measured by flow cytometry (FACSCanto II, BD, USA).

4.7. Mitochondrial Reactive Oxygen Species Examination

HT22 cells were co-cultured with Glioma261-mito-EGFP cells and then treated with 30 μg/mL CoNPs for 24 h. After centrifugation at 300 ×g, cells were incubated with 10 μM MitoSOX Deep Red working solution at 37°C in 5% CO_2 for 30 min. Mitochondrial superoxide levels were then measured by flow cytometry (FACSCanto II, BD, USA).

4.8. Mitochondrial Membrane Potential Determination

HT22 cells were co-cultured with Glioma261-mito-EGFP cells and then treated with 30 μg/mL CoNPs for 24 h. After washing, cells were incubated with 100 nM TMRE (tetramethylrhodamine ethyl ester) for 30 min at 37°C. Following two washes with pre-warmed PBS, fluorescence was acquired immediately using a FACSCanto II flow cytometer (excitation 561 nm, emission 582 nm).

4.9. Mdivi1 Concentration Determination

Cells were seeded in a 96-well plate at a density of 5×10^3 cells per well in 100 μL culture medium for 24 h, and then exposed to 0, 1, 2.5, 5, 10, 15, 20, 25, 30 μM Mdivi1 (a DRP1 inhibitor [30]) for 24 h. Then, 10 μL of CCK8 reagent (C0037, Beyotime, Shanghai, China) was added to each well and incubated at 37 ℃ for 1 h. Absorbance at 450 nm was measured using a microplate reader (Multiskan FC, Thermo Fisher Scientific, Waltham, MA, USA).

4.10. Quantitative real-time PCR

Total cellular RNA was isolated using TRIzol reagent according to the manufacturer's instructions. RNA concentration and purity (A_{260}/A_{280} ratio) were determined with a NanoDrop ND-1000 spectrophotometer. cDNA was prepared using the 1st Strand cDNA Synthesis Kit and assessed by quantitative real-time reverse transcription polymerase chain reaction (RT-PCR) using LightCycler 480 Real-Time PCR System (Roche, Switzerland). The $2^{-\Delta\Delta CT}$ method was used to calculate relative gene expression. Melting curve

analysis was performed to confirm amplicon specificity. Primer sequences used for amplification were as follows:

NR_030777 forward: 5’-TCTTACGGAGGTCTGGCATTC-3’ and reverse: 5’-CTCTTGCAGTAGCAATCGTCA-3’.

ACTB forward: 5’-GGCACAGTCAAGGCTGAGAATG-3’ and reverse: 5’-ATGGTGGTGAAGACGCCAGTA-3’.

4.11. Statistical analysis

Statistical analyses were performed using SPSS 20.0. All continuous data are presented as mean ± standard error of the mean (SEM). Shapiro–Wilk and Levene tests were first applied to confirm normality and homogeneity of variances, respectively. Differences among multiple groups were analyzed by one-way ANOVA followed by Tukey’s post-hoc test. For comparisons between two independent groups, an unpaired Student’s t-test was employed. When two factors were involved, two-way ANOVA with Bonferroni correction was used to assess main effects and interactions. All tests were two-tailed, and $P < 0.05$ was considered statistically significant.

Declarations

Competing interests

The authors declare that they have no competing interests.

Declaration of generative AI and AI-assisted technologies in the manuscript preparation process

During the preparation of this work the author(s) used Deepseek in order to polish the English language. After using this tool/service, the author(s) reviewed and edited the content as needed and take(s) full responsibility for the content of the published article.

Fundings

This work was supported by the National Natural Science Foundation of China (No. 81903352, 82473660), the Fujian Province Natural Science Foundation (No. 2025J09038, 2023J01316) and the Joint Funds for the Innovation of Science and Technology, Fujian province (No. 2025Y9266).

Author Contribution

Y.C. and X.C. wrote the main manuscript and performed investigation; X.L. and J.M.L. also investigated; Y.Z., Z.G., G.Y., H.H., and W.S. prepared figures; S.L. conducted software and formal analysis; S.W., H.L., and J.Z. supervised the work; F.Z. conceptualized, supervised, and wrote and revised the manuscript; S.J., C.C., L.L., and J.J.L. provided technical support. All authors reviewed the manuscript.

Acknowledgement

We appreciate S Zheng and Z Huang from the Public Technology Service Center, Fujian Medical University (Fuzhou, China) for their invaluable technical support.

Data Availability

The data are available upon request.

References

1. Grilli, M.L., et al., *Solutions for Critical Raw Materials under Extreme Conditions: A Review*. Materials (Basel), 2017. 10(3).
2. Tvermoes, B.E., et al., *Review of cobalt toxicokinetics following oral dosing: Implications for health risk assessments and metal-on-metal hip implant patients*. Crit Rev Toxicol, 2015. 45(5): p. 367–87.
3. Symanzik, C. and S.M. John, *Occupational exposure to cobalt nanoparticles: potential implications on risk assessment and preventive measures*. Br J Dermatol, 2023. 188(2): p. 161–162.
4. Harald, S., R. Kristín Vala, and K. Deniz, *Integrated Modelling of the Global Cobalt Extraction, Supply, Price and Depletion of Extractable Resources Using the WORLD6 Model.* Biophysical economics and resource quality, 2017.
5. Dahlstrand, H., et al., *Comparison of metal ion concentrations and implant survival after total hip arthroplasty with metal-on-metal versus metal-on-polyethylene articulations*. Acta Orthop, 2017. 88(5): p. 490–495.
6. Zheng, F., et al., *Cobalt induces neurodegenerative damages through Pin1 inactivation in mice and human neuroglioma cells*. J Hazard Mater, 2021. 419: p. 126378.
7. Julian, L.C. and A.I. Munoz, *Influence of microstructure of HC CoCrMo biomedical alloys on the corrosion and wear behaviour in simulated body fluids*. Tribology International, 2011. 44(3): p. 318–329.
8. Gilbert, J.L., et al., *In vivo oxide-induced stress corrosion cracking of Ti-6Al-4V in a neck-stem modular taper: Emergent behavior in a new mechanism of in vivo corrosion*. J Biomed Mater Res B Appl Biomater, 2012. 100(2): p. 584–94.
9. Gil, R.A. and A.I. Munoz, *Influence of the sliding velocity and the applied potential on the corrosion and wear behavior of HC CoCrMo biomedical alloy in simulated body fluids*. J Mech Behav Biomed Mater, 2011. 4(8): p. 2090–102.
10. Hawkins, S.J., et al., *Nanoparticle-induced neuronal toxicity across placental barriers is mediated by autophagy and dependent on astrocytes*. Nature Nanotechnology, 2018. 13(5): p. 427-+.
11. Zheng, F., et al., *Intercellular transfer of mitochondria via tunneling nanotubes protects against cobalt nanoparticle-induced neurotoxicity and mitochondrial damage*. Nanotoxicology, 2021. 15(10): p.

1358–1379.

12. Zheng, F., et al., *Comparison of the neurotoxicity associated with cobalt nanoparticles and cobalt chloride in Wistar rats*. Toxicol Appl Pharmacol, 2019. 369: p. 90–99.
13. Lin, X., et al., *ROS/mtROS promotes TNTs formation via the PI3K/AKT/mTOR pathway to protect against mitochondrial damages in glial cells induced by engineered nanomaterials*. Part Fibre Toxicol, 2024. 21(1): p. 1.
14. Li, J., et al., *NOX2 activation contributes to cobalt nanoparticles-induced inflammatory responses and Tau phosphorylation in mice and microglia*. Ecotoxicol Environ Saf, 2021. 225: p. 112725.
15. Chen, J., et al., *Cobalt nanoparticles induce mitochondrial damage and beta-amyloid toxicity via the generation of reactive oxygen species*. Neurotoxicology, 2023. 95: p. 155–163.
16. Chen, C., et al., *Evaluation of neurotoxicity and the role of oxidative stress of cobalt nanoparticles, titanium dioxide nanoparticles, and multiwall carbon nanotubes in Caenorhabditis elegans*. Toxicol Sci, 2023. 196(1): p. 85–98.
17. Grimm, A. and A. Eckert, *Brain aging and neurodegeneration: from a mitochondrial point of view*. J Neurochem, 2017. 143(4): p. 418–431.
18. Zheng, F., et al., *Intercellular transfer of mitochondria via tunneling nanotubes protects against cobalt nanoparticle-induced neurotoxicity and mitochondrial damage*. Nanotoxicology, 2022. 15(10): p. 1358–1379.
19. Rustom, A., et al., *Nanotubular highways for intercellular organelle transport*. Science, 2004. 303(5660): p. 1007–1010.
20. Delage, E., et al., *Differential identity of Filopodia and Tunneling Nanotubes revealed by the opposite functions of actin regulatory complexes*. Scientific Reports, 2016. 6.
21. Ahmad, T., et al., *Miro1 regulates intercellular mitochondrial transport & enhances mesenchymal stem cell rescue efficacy*. Embo Journal, 2014. 33(9): p. 994–1010.
22. Yang, H., et al., *LncRNA NR_030777 Alleviates Paraquat-induced Neurotoxicity by Regulating Zfp326 and Cpne5*. Toxicol Sci, 2020.
23. Esposito, R., et al., *Hacking the Cancer Genome: Profiling Therapeutically Actionable Long Non-coding RNAs Using CRISPR-Cas9 Screening*. Cancer Cell, 2019. 35(4): p. 545–557.
24. Peng, W.X., P. Koirala, and Y.Y. Mo, *LncRNA-mediated regulation of cell signaling in cancer.* Oncogene, 2017. 36(41): p. 5661–5667.
25. Briggs, J.A., et al., *Mechanisms of Long Non-coding RNAs in Mammalian Nervous System Development, Plasticity, Disease, and Evolution*. Neuron, 2015. 88(5): p. 861–877.
26. Chen, N., et al., *LncRNA NR_030777 promotes mitophagy by targeting CDK1-related mitochondrial fission and ATG12 to attenuate paraquat-induced Parkinson's disease.* Environ Pollut, 2024: p. 123875.
27. Wang, J., et al., *The interplay between lncRNA NR_030777 and SF3B3 in neuronal damage caused by paraquat*. Ecotoxicol Environ Saf, 2023. 255: p. 114804.

28. Hagiwara, F., et al., *Brain Delivery of Cisplatin Using Microbubbles in Combination with Ultrasound as an Effective Therapy for Glioblastoma*. Pharmaceuticals (Basel), 2023. 16(11).
29. Abounit, S., E. Delage, and C. Zurzolo, *Identification and Characterization of Tunneling Nanotubes for Intercellular Trafficking*. Current Protocols in Cell Biology, 2015. 67(1).
30. Deng, Y., et al., *Mdivi-1, a mitochondrial fission inhibitor, reduces angiotensin-II- induced hypertension by mediating VSMC phenotypic switch*. Biomed Pharmacother, 2021. 140: p. 111689.
31. Herdy, J.R., J. Mertens, and F.H. Gage, *Neuronal senescence may drive brain aging*. Science, 2024. 384(6703): p. 1404–1406.
32. Li, J., Z. Xuan, and C. Liu, *Long non-coding RNAs and complex human diseases*. Int J Mol Sci, 2013. 14(9): p. 18790–808.
33. Ma, X., et al., *Ubiquitination and Long Non-coding RNAs Regulate Actin Cytoskeleton Regulators in Cancer Progression*. Int J Mol Sci, 2019. 20(12).
34. Kopp, F. and J.T. Mendell, *Functional Classification and Experimental Dissection of Long Noncoding RNAs*. Cell, 2018. 172(3): p. 393–407.
35. Yang, H., et al., *LncRNA NR_030777 Alleviates Paraquat-Induced Neurotoxicity by Regulating Zfp326 and Cpne5*. Toxicol Sci, 2020. 178(1): p. 173–188.
36. Liu, J., et al., *Metallic cobalt nanoparticles imbedded into ordered mesoporous carbon: A non-precious metal catalyst with excellent hydrogenation performance*. J Colloid Interface Sci, 2017. 505: p. 789–795.
37. Liu, K., et al., *Mesenchymal stem cells rescue injured endothelial cells in an in vitro ischemia-reperfusion model via tunneling nanotube like structure-mediated mitochondrial transfer*. Microvasc Res, 2014. 92: p. 10–8.
38. Han, H., et al., *Bone marrow-derived mesenchymal stem cells rescue injured H9c2 cells via transferring intact mitochondria through tunneling nanotubes in an in vitro simulated ischemia/reperfusion model*. Molecular medicine reports, 2016. 13(2): p. 1517–1524.
39. Li, X., et al., *Mitochondrial transfer of induced pluripotent stem cell-derived mesenchymal stem cells to airway epithelial cells attenuates cigarette smoke-induced damage*. Am J Respir Cell Mol Biol, 2014. 51(3): p. 455–465.
40. Yang, Y., et al., *Transfer of mitochondria from mesenchymal stem cells derived from induced pluripotent stem cells attenuates hypoxia-ischemia-induced mitochondrial dysfunction in PC12 cells*. Neural Regen Res, 2020. 15(3): p. 464–472.
41. Deng, P., et al., *Long-term cadmium exposure impairs cognitive function by activating lnc-Gm10532/m6A/FIS1 axis-mediated mitochondrial fission and dysfunction*. Sci Total Environ, 2023. 858(Pt 3): p. 159950.
42. Deng, L., et al., *Long Non-coding RNA ANRIL Downregulation Alleviates Neuroinflammation in an Ischemia Stroke Model via Modulation of the miR-671-5p/NF-κB Pathway*. Neurochem Res, 2022. 47(7): p. 2002–2015.

Figures

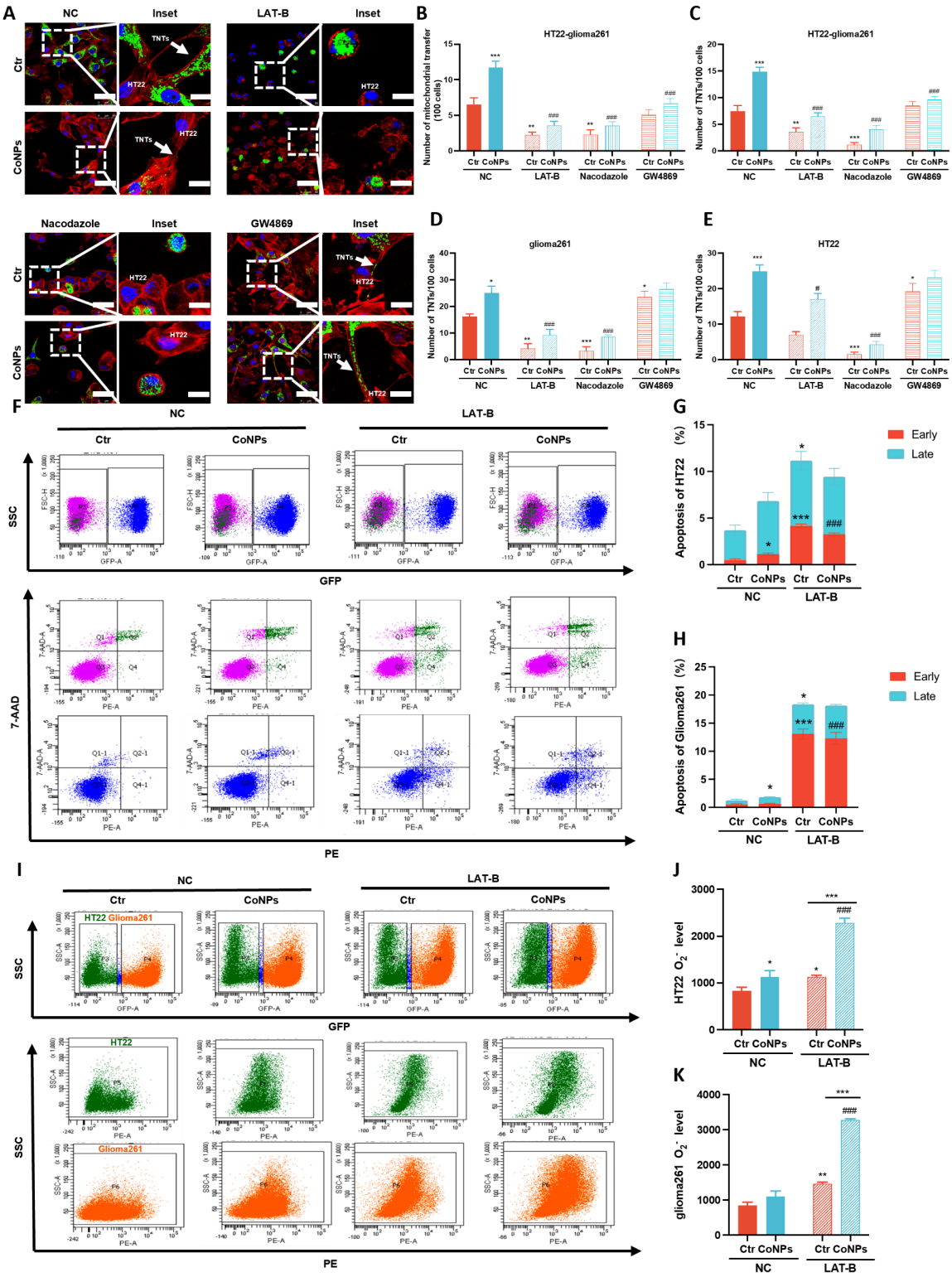


Figure 1

Inhibition of TNTs exacerbated CoNPs-induced neuronal damage, as shown by reduced mitochondrial transfer, increased apoptosis, and elevated O_2^- generation in HT22 and Glioma261 co-cultures. (A) Representative images of HT22 and Glioma261 co-cultures treated with CoNPs for 24 h. **(B)**

Quantification of mitochondrial transfer from Glioma261 to HT22. **(C)** The number of heterotypic TNTs between Glioma261 and HT22. **(D)** The number of homotypic TNTs between Glioma261. **(E)** The number of homotypic TNTs between HT22. Scale bar = 50 μm, inset scale bar = 25 μm. **(F)** Apoptosis analysis of both cell types after CoNPs treatment in the co-culture system with or without LAT-B. **(G-H)** Statistical graphs of **(F)**. **(I)** Cellular O_2^- level of the two cells after CoNPs treatment in the co-culture system for 24 h. **(J-K)** Statistical graphs of **(I)**. compared with control group, **P*<0.05, ***P*<0.01, ****P*<0.001; compared with the CoNPs group, #*P*<0.05, ### *P*<0.001. n = 3.

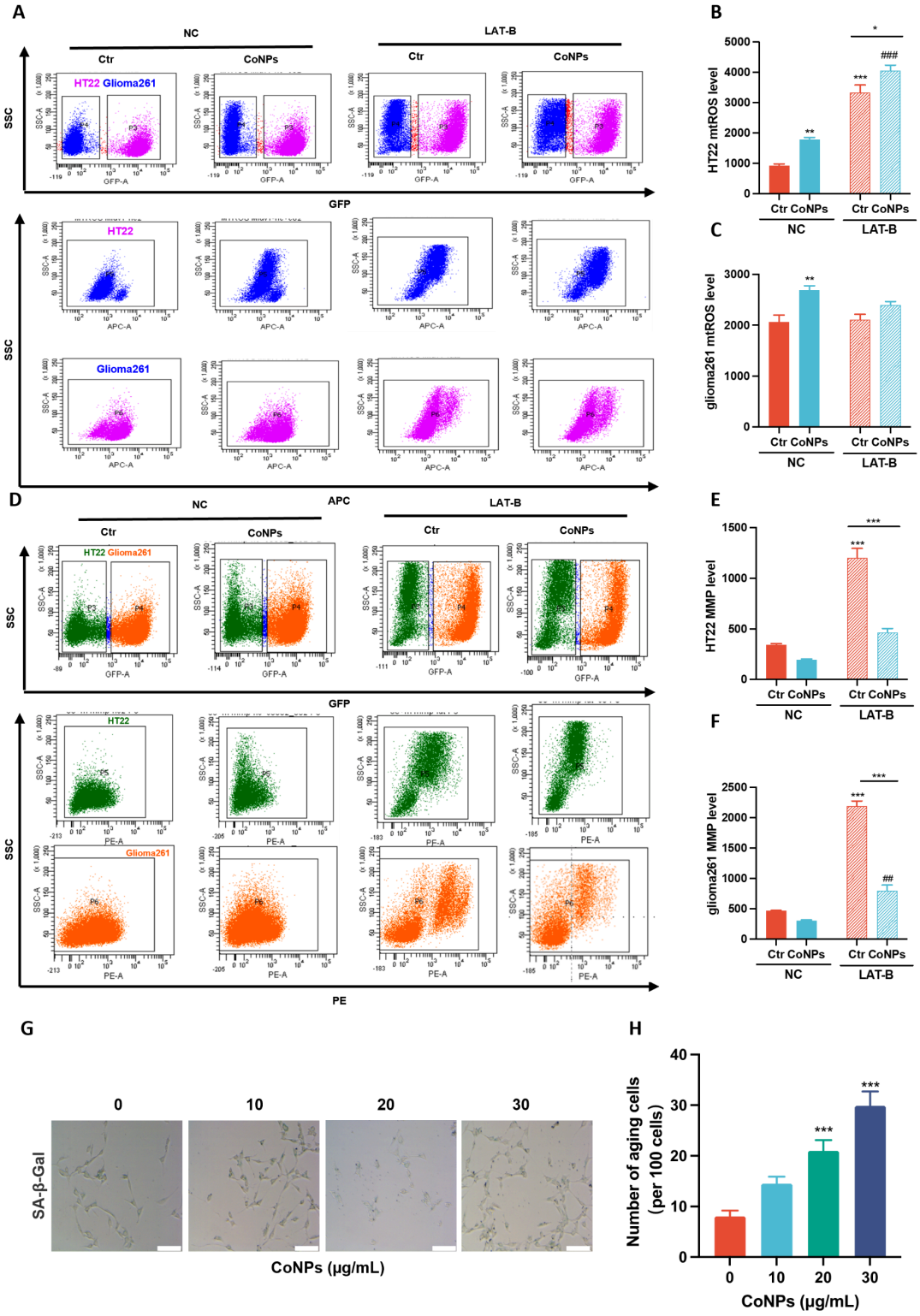


Figure 2

TNTs-mediated mitochondrial transfer modulated CoNPs-induced mitochondrial dysfunction and cellular senescence. (A) Mitochondrial reactive oxygen species in two cells after CoNPs treatment in HT22 and Glioma261 co-culture system for 24 h. **(B-C)** Statistical graphs of **(A)**. **(D)** MMP in two cells after CoNPs treatment in co-culture system of HT22 and Glioma261 for 24 h, **(E-F)** Statistical graphs of **(D)**. **(G)** The levels of SA-β-Gal in HT22 after CoNPstreatment for 24 h. Scale bar = 10 μm. **(H)** The

number of aging cells in HT22. Compared with the control group, *P<0.05, **P<0.01, ***P<0.001; Compared with CoNPs group, ## P<0.01, ### P<0.001. n = 3.

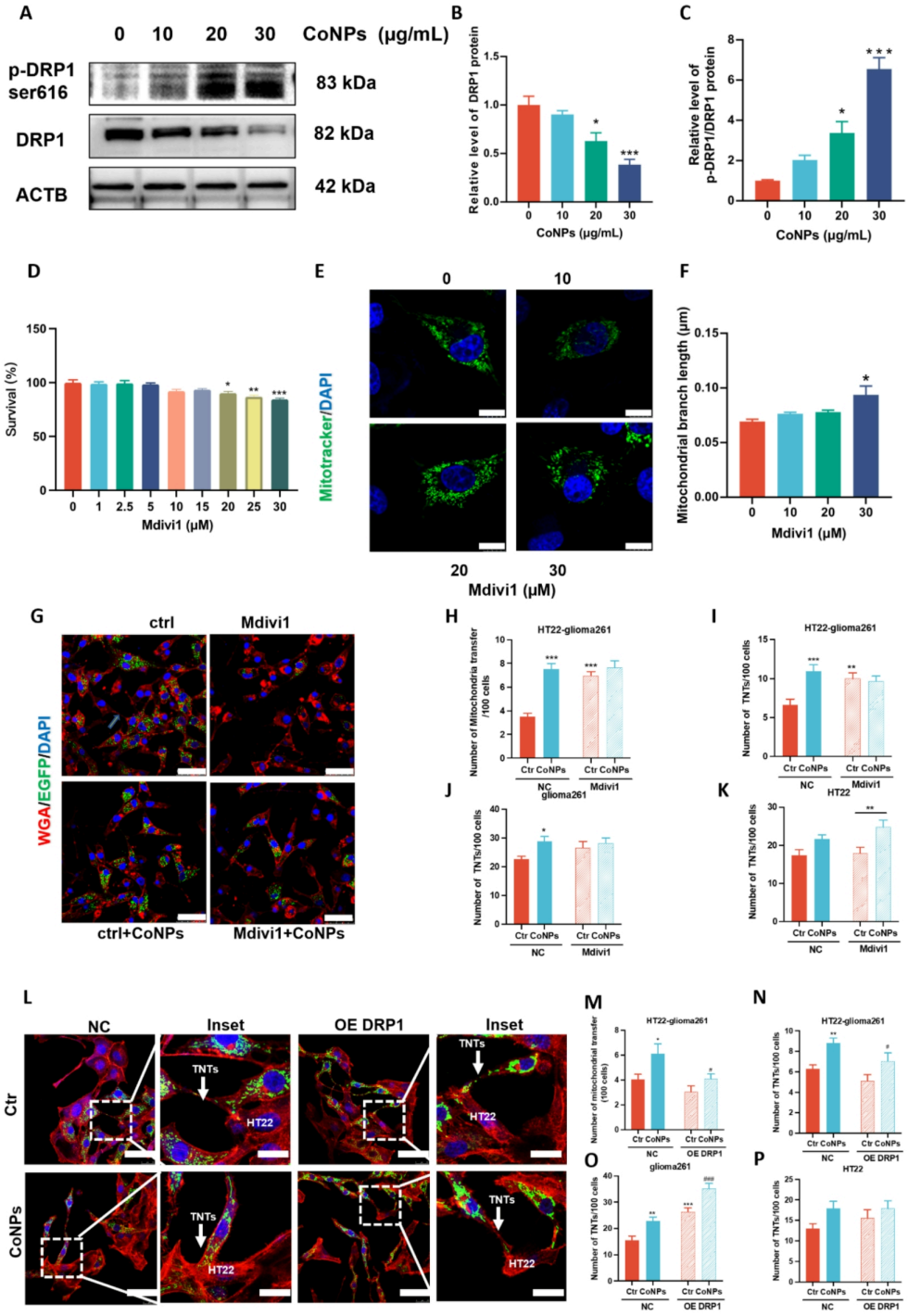


Figure 3

CoNPs suppressed DRP1 expression to promote TNTs formation and mitochondrial transfer. (A) Protein levels of DRP1 and p-DRP1 (Ser616) in Glioma261 after treatment with CoNPs for 24 h. **(B-**

C)Quantification of the protein levels shown in **(A)**. **(D)** Cell viability of Glioma261 after 24 h treatment with the DRP1 inhibitor Mdivi-1. **(E)**Mitochondrial morphology in Glioma261 following 24h treatment to Mdivi-1. Scale bar = 10 μm. (**F)** Quantification of mitochondrial branch length corresponding to **(E)**. **(G)** Representative images of Glioma261 co-cultured with HT22 for 24 h after Mdivi-1 pretreatment. **(H)** Number of mitochondria transferred from Glioma261 to HT22 after DRP1 inhibition. **(I)**Number of TNTs formed between Glioma261 and HT22 under DRP1 inhibition. **(J)**Number of TNTs observed between Glioma261 cells following DRP1 suppression. **(K)**Number of TNTs among HT22 after DRP1 inhibition in Glioma261. **(L)** Representative micrographs of DRP1-overexpressing Glioma261 co-cultured with HT22 for 24 h. **(M)** Number of mitochondria transferred from Glioma261 to HT22 under DRP1 overexpression conditions. **(N)** Number of TNTs formed between Glioma261 and HT22 following DRP1 overexpression. **(O)** Number of TNTs observed among Glioma261 after DRP1 overexpression. **(P)** Number of TNTs detected between HT22 under DRP1 overexpression in Glioma261.Scale bar = 50 μm. inset scale bar = 25 μm. compared with the control group, **P*<0.05, ***P*<0.01, ****P*<0.001; compared with the CoNPs group, #*P*<0.05, ### *P*<0.001. n = 3.

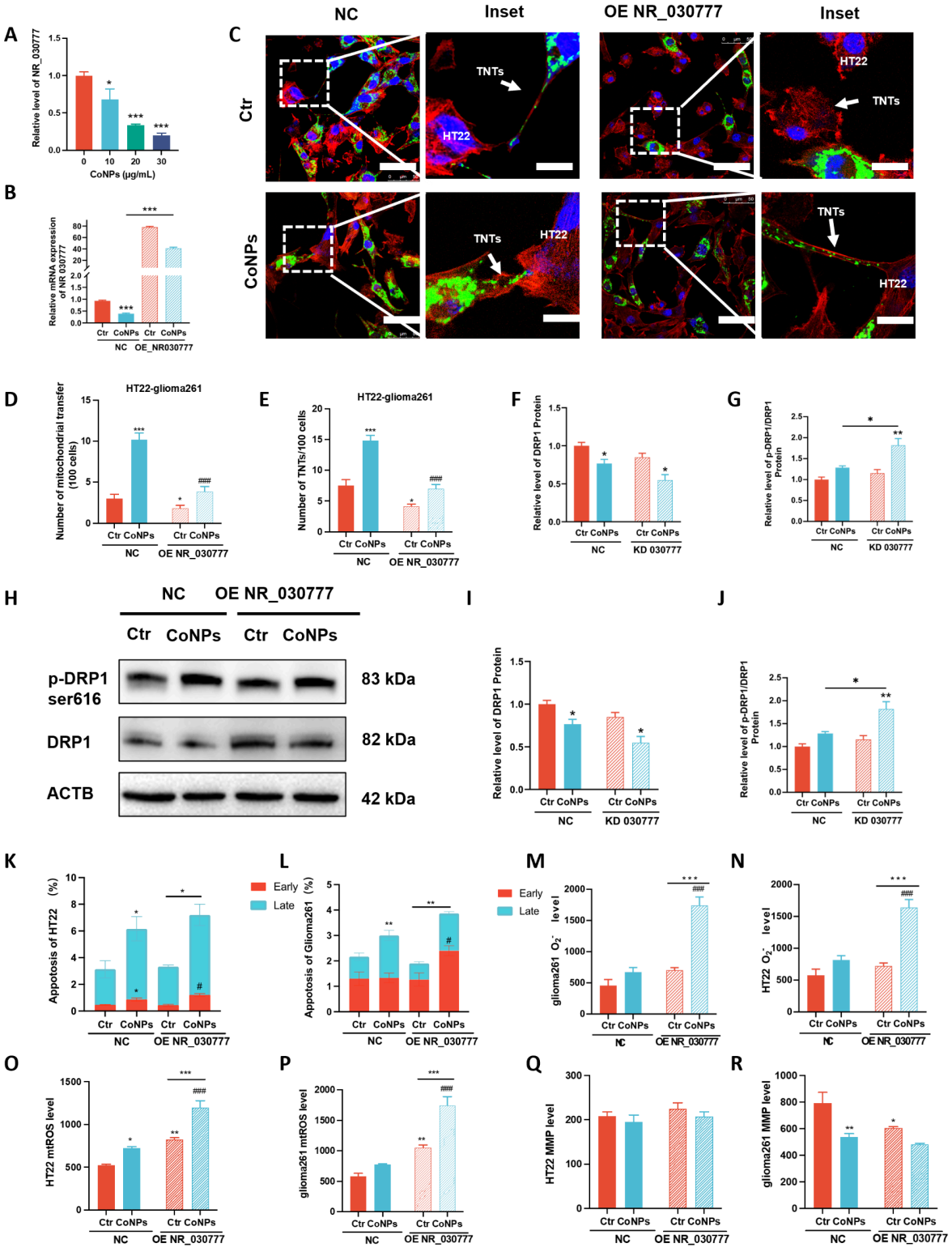


Figure 4

NR_030777 overexpression impaired TNTs-mediated mitochondrial transfer and exacerbates CoNPs-induced cytotoxicity in Glioma261 and HT22 co-culture. (A) Expression levels of NR_030777 after CoNPs treatment of Glioma261 for 24 h. **(B)**Successful construction of plasmid overexpression Glioma261 NR_030777 model. **(C)**Representative images of the co-culture of NR_030777-overexpressing Glioma261 and HT22 for 24 h. **(D)** The number of mitochondria transferred from NR_030777-

overexpressing Glioma261 to HT22. **(E)** The number of TNTs between NR_030777-overexpressing Glioma261 and HT22. **(F)** The number of TNTs between homotypic NR_030777-overexpressing Glioma261 cells. **(G)** The number of TNTs between HT22 cells. **(H)** Protein levels of DRP1 and p-DRP1 (Ser616) in NR_030777-overexpressing Glioma261 following 24 h CoNPs treatment. **(I-J)**Statistical graphs of **(H)**. **(K-L)** Statistical graphs of apoptosis in HT22 and NR_030777-overexpressing Glioma261 after 24 h co-culture with CoNPs treatment. **(M-N)** Statistical graphs of O_2^- levels in HT22 and NR_030777-overexpressing Glioma261 after 24 h co-culture with CoNPs treatment. **(O-P)**Statistical graphs of mitoROS levels in HT22 and NR_030777-overexpressing Glioma261 after 24 h co-culture with CoNPs treatment. **(Q-R)** Statistical graphs of MMP of the two cell groups after 24 h in Glioma261 NR_030777 co-culture system. The original multicolor flow cytometry dot plots are presented in **Supplementary Figure S1**. Scale bar = 50 μm, inset scale bar = 25 μm. Compared with the control group, **P*<0.05, ***P*<0.05, ****P*<0.05; compared with the CoNPs group, #*P*<0.05, ## *P*<0.01, ###*P*<0.001. n = 3.

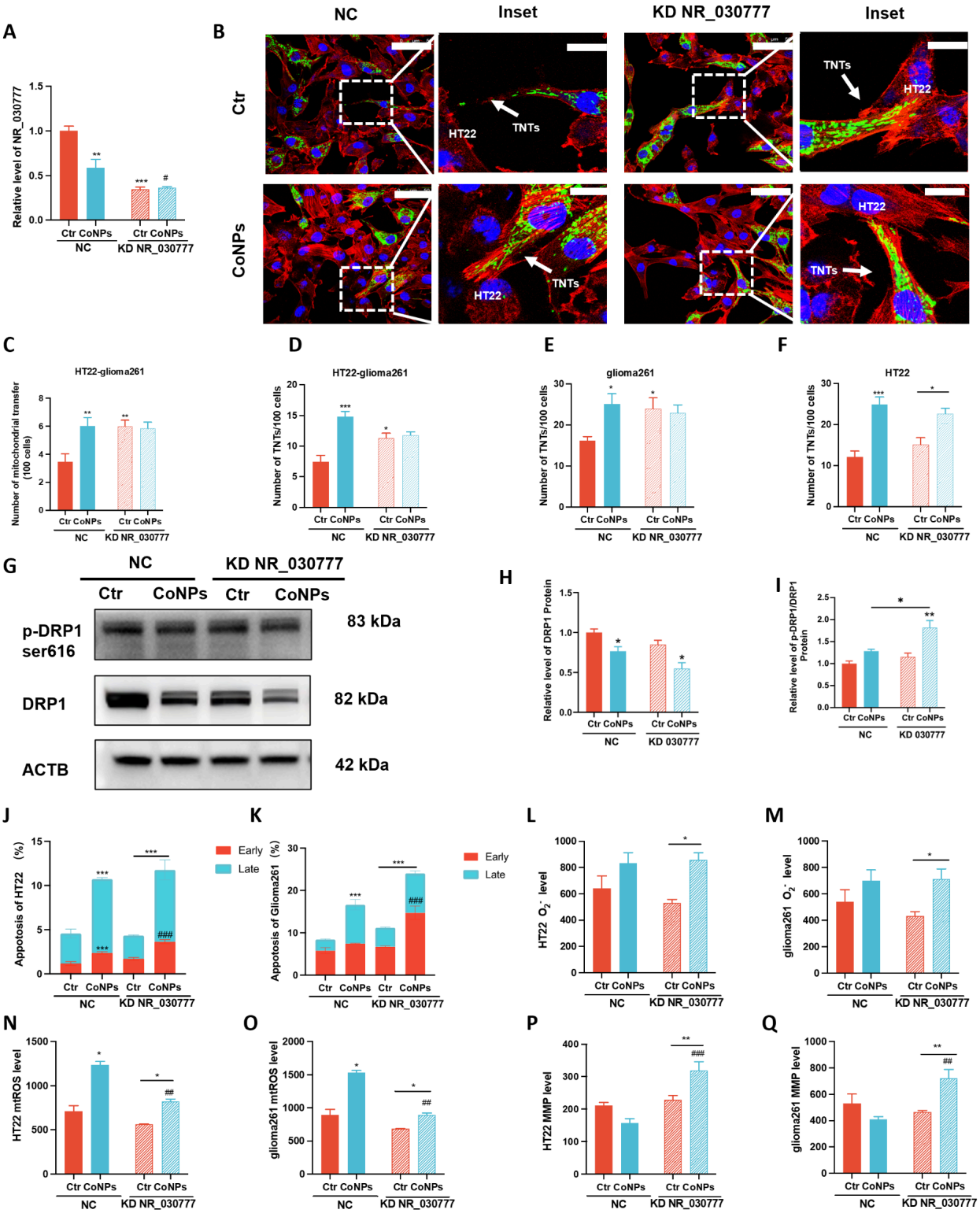


Figure 5

NR_030777 knockdown in Glioma261 cells impaired TNT-mediated mitochondrial transfer to HT22 cells and modulated oxidative stress response induced by CoNPs.

(A) Successful construction of NR_030777 knockdown Glioma261 using siRNA. **(B)** Representative mitochondrial transfer images of co-culture of NR_030777-knockdown Glioma261 and HT22 for 24 h. **(C)**

The number of mitochondria transferred from NR_030777-knockdown Glioma261 to HT22. **(D)** The number of TNTs between NR_030777-knockdown Glioma261 and HT22. **(E)** The number of TNTs between homotypic NR_030777-knockdown Glioma261 cells. **(F)** The number of TNTs between HT22 cells. **(G-H)** Quantitative analysis of DRP1 and p-DRP1 (Ser616) protein levels shown in (G)**. (J-K)**Apoptosis levels in both cell populations in the co-culture system of HT22 and NR_030777-knockdown Glioma261 treated with CoNPs for 24 h. **(L-M)**Intracellular O_2^- levels in co-culture system after 24 h. **(N-O)** mtROS in HT22 and NR_030777-knockdown Glioma261 co-cultures following 24 h CoNPs treatment. **(P-Q)** MMP in co-culture system after 24 h CoNPs treatment. The original multicolor flow cytometry dot plots are presented in **Supplementary Figure S2**. Scale bar = 50 μm, inset scale bar = 25 μm. Compared with the control group; **P*<0.05, ***P*<0.05, ****P*<0.05; compared with the CoNPs group, #*P*<0.05, ## *P*<0.01, ###*P*<0.001. n = 3.

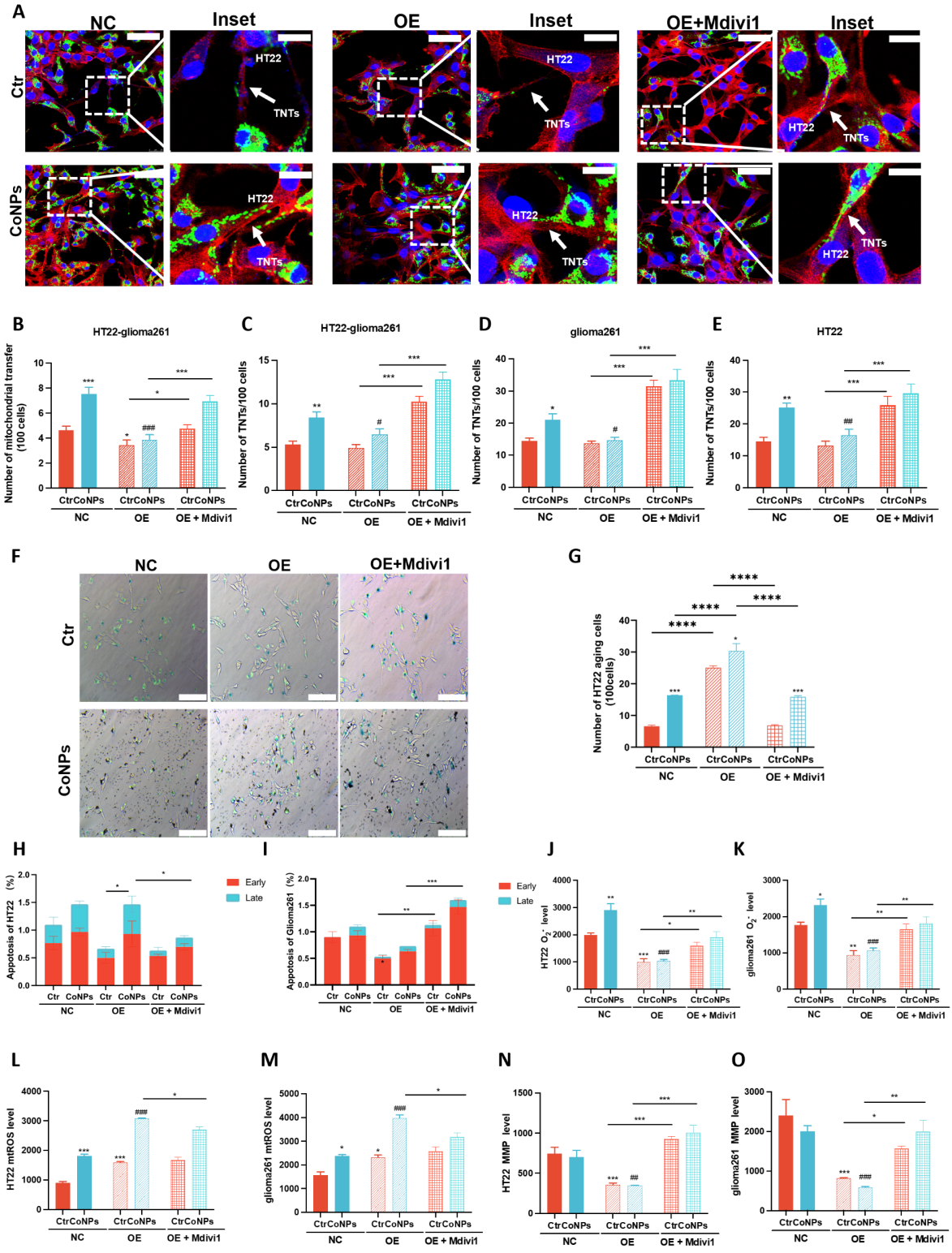


Figure 6

Overexpression of lncRNA NR_030777 in glial cells suppressed DRP1-mediated mitochondrial transfer via TNTs and exacerbated CoNPs-induced oxidative stress and mitochondrial dysfunction. (A) Representative images of co-culture of NR_030777-overexpressing Glioma261 treated with DRP1 inhibitor Mdivi-1, co-cultured with HT22 for 24 h. **(B)** Quantification of mitochondria transferred from NR_030777-overexpressing Glioma261 with DRP1 inhibition to HT22. **(C)** Number of TNTs between

NR_030777-overexpressing Glioma261 (with DRP1 inhibition) and HT22. **(D)** Number of TNTs among homotypic NR_030777-overexpressing Glioma261 cells with DRP1 inhibition. **(E)**The number of TNTs between HT22 cells. **(F)** SA-β-gal staining of co-culture of NR_030777-overexpressing Glioma261 (with DRP1 inhibition) and HT22 for 24 h. Scale bar = 100 μm. **(G)** Quantification of SA-β-gal-positive senescent cells in Glioma261. **(H-I)**Apoptosis levels in HT22 and NR_030777-overexpressing Glioma261 with DRP1 inhibition after 24 h co-culture and CoNPs treatment, respectively. **(J-K)**Intracellular O_2^- levels of the two cell types under the same conditions. **(L-M)**Statistical graphs of mtROS were treated with CoNPs in HT22 and overexpressing Glioma261 NR_030777 and inhibited DRP1 co-culture system for 24 h. **(N-O)**Statistical graphs of MMP under the same conditions. The original multicolor flow cytometry dot plots are presented in **Supplementary Figure S3-4**. Scale bar = 50 μm, inset scale bar = 25 μm. Compared with the control group, **P*<0.05, ***P*<0.05, ****P*<0.05; compared with the CoNPs group, #*P*<0.05, ## *P*<0.01, ###*P*<0.001. n = 3.

Supplementary Files

This is a list of supplementary files associated with this preprint. Click to download.

- SupplementaryMaterial.docx
- floatimage7.png